Atomic-scale structure of nanocrystalline ZrO_2 prepared by high-energy ball milling

M. Gateshki and V. Petkov*
Department of Physics, Central Michigan University, Mt. Pleasant, Michigan 48859, USA

G. Williams
Department of Biology, Central Michigan University, Mt. Pleasant, Michigan 48859, USA

S. K. Pradhan
Department of Physics, The University of Burdwan, Golapbag, Burdwan-713104, West Bengal, India

Y. Ren
Advanced Photon Source, Argonne National Laboratory, Argonne, Illinois 60439, USA
(Received 12 December 2004; revised manuscript received 14 March 2005; published 21 June 2005)

The atomic-scale structure of nanocrystalline ZrO_2 obtained by ball milling has been studied using high-energy x-ray diffraction and the atomic pair distribution function technique. The studies show that, upon relatively short milling times, the parent crystalline material, monoclinic ZrO_2, evolves into a nanocrystalline phase that is locally similar to monoclinic zirconia but shows a cubic-type ordering at nanometer-range distances. The result underlines the importance of local structural distortions in stabilizing the technologically important cubic zirconia at room temperature.

DOI: 10.1103/PhysRevB.71.224107 PACS number(s): 61.10.Nz, 81.07.Bc

I. INTRODUCTION

Zirconia possesses a unique combination of mechanical and electrical properties making it very useful in applications, such as heat insulators, oxygen sensors, fuel cells, and catalyst supports.[1] At atmospheric pressure, pure ZrO_2 is known to adopt three different crystal structures. At high temperature (>2640 K), it has a cubic structure (space group $Fm\bar{3}m$). Between 1440 K and 2640 K, zirconia is tetragonal ($P4_2/nmc$), and below 1440 K—monoclinic ($P2_1/c$). The tetragonal-to-monoclinic phase transition is accompanied by a 3–5% volume increase which causes cracking of bulk zirconia samples and, hence, the deterioration of the material's mechanical properties. This renders pure zirconia virtually useless for technological applications. To remedy the problem, the high-temperature phases (tetragonal or cubic) of zirconia are stabilized at room temperature by doping the material with Mg, Ca, Sc, Y, or Nd.[2,3] The doping quenches the cubic/tetragonal-to-monoclinic phase transition and the associated mechanical strain, but the material's properties are still impaired for some applications.[4] Another approach for stabilizing the high-temperature phases at room temperature is via reducing the crystallite size to a few nanometers.[4–11] Several different routes have been proposed for producing nanocrystalline zirconia: Heat treatment of amorphous $ZrO(OH)_2$;[4] sol-gel method using zirconium *n*-butoxide as a precursor;[9] spray-pyrolysis technique using a water solution of $ZrO(NO_3)_2$ (Ref. 10), and high-energy ball milling.[6,11] The latest technique has gained particular popularity due to its ease of use and ability to produce large quantities at low cost. Although traditional techniques for structure determination have shown that the high-temperature phases (either tetragonal or cubic) are stabilized in nanocrystalline zirconia prepared by ball milling, some controversy about the type of atomic structure and phase content has arisen. For example, Gaffet *et al.*[8] and Chadwick *et al.*[11] have observed a formation of tetragonal and amorphous phases in nanocrystalline zirconia obtained by ball milling. On the other hand, Bid *et al.*[6] have observed a mixture of monoclinic and cubic phases. A detailed and accurate knowledge about the atomic ordering is important for a better understanding of the material's properties. Here, we report results from a structural study of nanocrystalline ZrO_2 obtained by ball milling. We employ high-energy x-ray diffraction (XRD) and the atomic pair distribution function (PDF) technique. This allows us to obtain information both for the average (nanometer-range distances) and local (subnanometer-range distances) atomic ordering with very good spatial resolution. We find that the average structure of nanocrystalline zirconia may well be described in terms of a cubic lattice and periodicity, while locally the material is less ordered and resembles the monoclinic phase of ZrO_2 crystals.

II. EXPERIMENTAL SECTION

A. Sample preparation

Nanocrystalline zirconia was obtained by high-energy milling of crystalline ZrO_2 with monoclinic symmetry (Z-Tech, Australia, SF-ULTRA, high purity = 99.97%). The milling was conducted in a planetary mill (Model P5, Fritsch Gmbh, Germany) carrying vials rotating with a speed of 450 rpm. The vials contained 30 hardened chrome steel balls with a diameter of 10 mm, ensuring a ball-to-powder mass ratio of 40:1. In order to reveal the steps in the transformation of monoclinic zirconia to a nanophase material, we prepared and investigated five samples milled for times of 1, 3, 5, 8, and 12 h. The as-prepared samples were sealed between thin

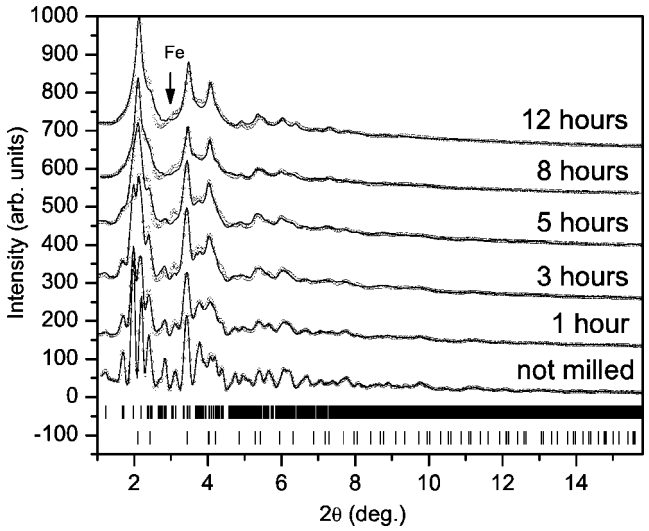

FIG. 1. Experimental powder diffraction patterns (symbols) for ZrO_2 samples milled for different times and calculated patterns (lines) obtained through two-phase Rietveld refinements. The positions of the Bragg peaks of the monoclinic (the upper set of bars) and cubic (the lower set of bars) phases are given in the lower part of the plot. The weak peak at $2\theta = 3.1°$ in the XRD pattern of the milled samples is due to body-centered-cubic Fe from the steel container and balls. Microanalysis performed by us and other authors (Ref. 8) indicate that iron is isolated in small particles and not incorporated in the milled material.

Kapton foils and subjected to synchrotron radiation diffraction experiments.

B. Synchrotron radiation diffraction experiments

XRD experiments were carried out at the beamline 11-ID-C (Advanced Photon Source, Argonne National Laboratory) using x-rays of energy 114.496 keV ($\lambda = 0.1083$). A Si standard was used to cross check the x-ray energy calibration and beamline optics alignment. The high-energy x-rays were used to obtain diffraction data to higher values of the wave vector, Q, which is important for the success of PDF analysis. The measurements were carried out in symmetric transmission geometry, and scattered radiation was collected with an intrinsic germanium detector connected to a multichannel analyzer. Several runs were conducted with each of the samples and the resulting XRD patterns were averaged to improve the statistical accuracy and reduce any systematic effect due to instabilities in the experimental setup. The diffraction patterns obtained are shown in Fig. 1. As can be seen, the XRD pattern of monoclinic (not milled) zirconia exhibits well-defined Bragg peaks up to $Q \sim 8$–10 Å^{-1}. The material is obviously a perfect crystalline solid. The Bragg peaks in the XRD patterns of the milled samples are rather broad, and merge into a slowly oscillating diffuse component already at Q values as low as 4–5 Å^{-1}. Such diffraction patterns are typical for materials of limited structural coherence and are very difficult to tackle by traditional techniques for structure determination. However, when reduced to the corresponding atomic PDFs, they become a structure-sensitive quantity lending itself to structure determination.

The atomic PDF, $G(r)$, is defined as follows:

$$G(r) = 4\pi r[\rho(r) - \rho_0], \tag{1}$$

where $\rho(r)$ and ρ_0 are the local and average atomic number densities, respectively, and r is the radial distance. It peaks at characteristic distances separating pairs of atoms and thus reflects the atomic-scale structure. The PDF $G(r)$ is the Fourier transform of the experimentally observable total structure function, $S(Q)$, i.e.,

$$G(r) = (2/\pi)\int_{Q=o}^{Q_{\max}} Q[S(Q) - 1]\sin(Qr)dQ, \tag{2}$$

where Q is the magnitude of the wave vector ($Q = 4\pi \sin\theta/\lambda$), 2θ is the angle between the incoming and outgoing radiation beams, and λ is the wavelength of the radiation used. The structure function is related to the coherent part of the total scattered intensity as follows:

$$S(Q) = 1 + \left[I^{\mathrm{coh}}(Q) - \sum c_i|f_i(Q)|^2\right]/\left|\sum c_i f_i(Q)\right|^2, \tag{3}$$

where $I^{\mathrm{coh}}(Q)$ is the coherent scattering intensity per atom in electron units and c_i and f_i are the atomic concentration and x-ray scattering factor, respectively, for the atomic species of type i.[12,13] As can be seen from Eqs. (1)–(3), the PDF is simply another representation of the powder diffraction data. However, exploring the diffraction data in real space is advantageous, especially in the case of materials of limited structural coherence. First, as Eqs. (2) and (3) imply, the *total* scattering, including Bragg scattering as well as diffuse scattering, contributes to the PDF. In this way, both the average longer-range atomic structure—manifested in the sharp Bragg peaks—and the local structural imperfections—manifested in the diffuse component of the diffraction pattern—are reflected in the PDF. Second, by accessing high values of Q, experimental PDFs with improved real-space resolution can be obtained and hence, quite fine structural features can be revealed.[14] In fact, data at high Q values ($Q > 10$ Å^{-1}) are critical for the success of PDF analysis. Third, the PDF is less affected by diffraction optics and experimental factors since these are accounted for in the step of extracting the coherent intensities from the raw diffraction data. This renders the PDF a structure-dependent quantity that directly gives the relative positions of atoms in materials. As demonstrated previously,[15–17] this enables convenient testing and refinement of structural models.

Experimental PDFs for the studied samples were obtained as follows. First, the coherently scattered intensities were extracted from the XRD patterns, shown in Fig. 1, by applying appropriate corrections for flux, background, Compton scattering, and sample absorption. The intensities were normalized in absolute electron units, reduced to structure functions $Q[S(Q)-1]$ and Fourier transformed to atomic PDFs. Thus obtained experimental atomic PDFs are shown in Fig. 2. All data processing was done with the help of the program RAD.[18]

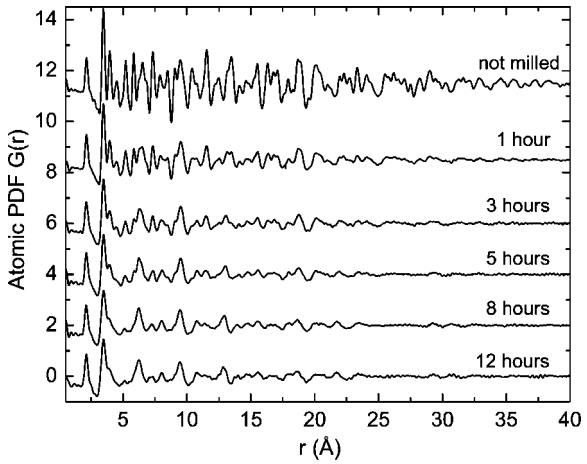

FIG. 2. Atomic PDFs obtained from the powder diffraction patterns of Fig. 1.

III. RESULTS

As can be seen in Fig. 2, the experimental PDF for crystalline (not milled) ZrO_2 is rich in well-defined structural features extending to high real-space distances, as it should be with a material possessing a long-range atomic order. The PDFs for the ball-milled samples are also rich in well-defined features but they vanish already at 20 Å. Obviously, those samples have an atomic arrangement very well defined at nanoscale distances, but lack the extended order of usual crystals. On the other hand, transmission electron microscopy (TEM) studies (Fig. 3) show that the average grain size of the milled samples is of the order of 250–400 nm. These two experimental observations suggest that the decay of the experimental PDFs of the nanocrystalline samples at higher interatomic distances [$G(r) \sim 0$ at approximately (approx.) 2–3 nm] is caused not by small grain size but by local structural disorder, which limits the structural coherence to approx. 2–3 nm. In this respect, the samples milled for longer times (longer than 5 h) may be considered as nanocrystalline in nature. The relatively large size of the grains also means that the surface energy, which can contribute substantially to the stabilization of a particular phase in a nanocrystalline material,[4,5,10] will have a negligible effect in our case.

FIG. 3. TEM image of nanocrystalline zirconia (12 h milled sample).

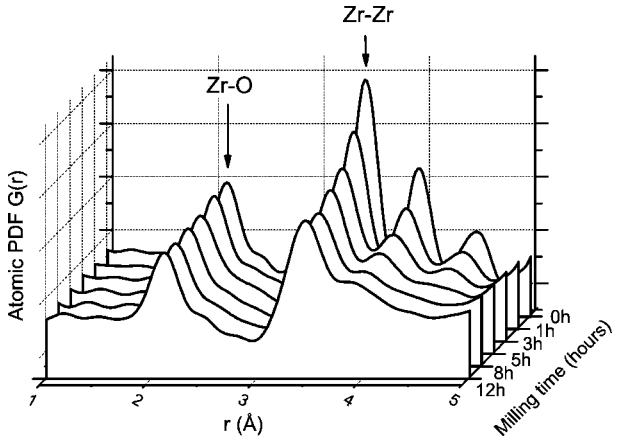

FIG. 4. Low-*r* part of the experimental PDFs of Fig. 2. Reflecting the monoclinic-type local atomic ordering the first PDF peak (Zr–O atomic pairs) is positioned at approx. 2.13 Å, and the second one (Zr–Zr atomic pairs) at ~3.46 Å. Note that the first-neighbor Zr–O and Zr–Zr distances in cubic zirconia are 2.22 Å and 3.63 Å, respectively, and this is not what our PDF data show.

A careful inspection of Figs. 1 and 2 shows a considerable change in the experimental data with milling time. The changes are especially noticeable in the higher-*r* region (5–20 Å) of the PDF data. The peaks in the PDFs of the milled samples become less pronounced (signaling increased structural disorder) and diminish in number with milling time. The latter observation signals the onset of a structural phase transition leading to a nanophase of increased symmetry (i.e., of a phase with a diminished number of distinct interatomic distances/coordination spheres). On the other hand, the positions and the shapes of the low-*r* ($r < 5$ Å) peaks in the experimental PDFs hardly show any change with milling time. Those peaks are shown in Fig. 4 on an expanded scale. The first peak (~2.13 Å) corresponds to the first neighbor Zr–O and the second peak (~3.46 Å)—to the first neighbor Zr–Zr distances. As the data in Figs. 4 and 5 clearly show, these distances hardly change when crystalline zirconia is turned into nanocrystalline. The number of first-neighbor Zr-O atomic pairs, which is proportional to the area under the first PDF peak, hardly changes too. Similar results have been obtained by independent x-ray absorption fine structure.[7,11] What changes is the broadening of the peaks reflecting an increased local structural disorder. But that increase is limited and does not scale with the milling time as the data in Fig. 5(b) show. These observations indicate that the local atomic ordering of monoclinic ZrO_2 is, to a great extent, preserved in the nanocrystalline zirconia obtained by it. Thus, the results of the preliminary analysis of the experimental data suggest a somewhat unusual picture: A nanophase material with atomic arrangement that is locally less ordered than it is on longer-range distances.

IV. DISCUSSION

To reveal the three-dimensional (3D) atomic ordering in nanocrystalline zirconia in more detail, we tested several structural models by fitting them to the experimental diffrac-

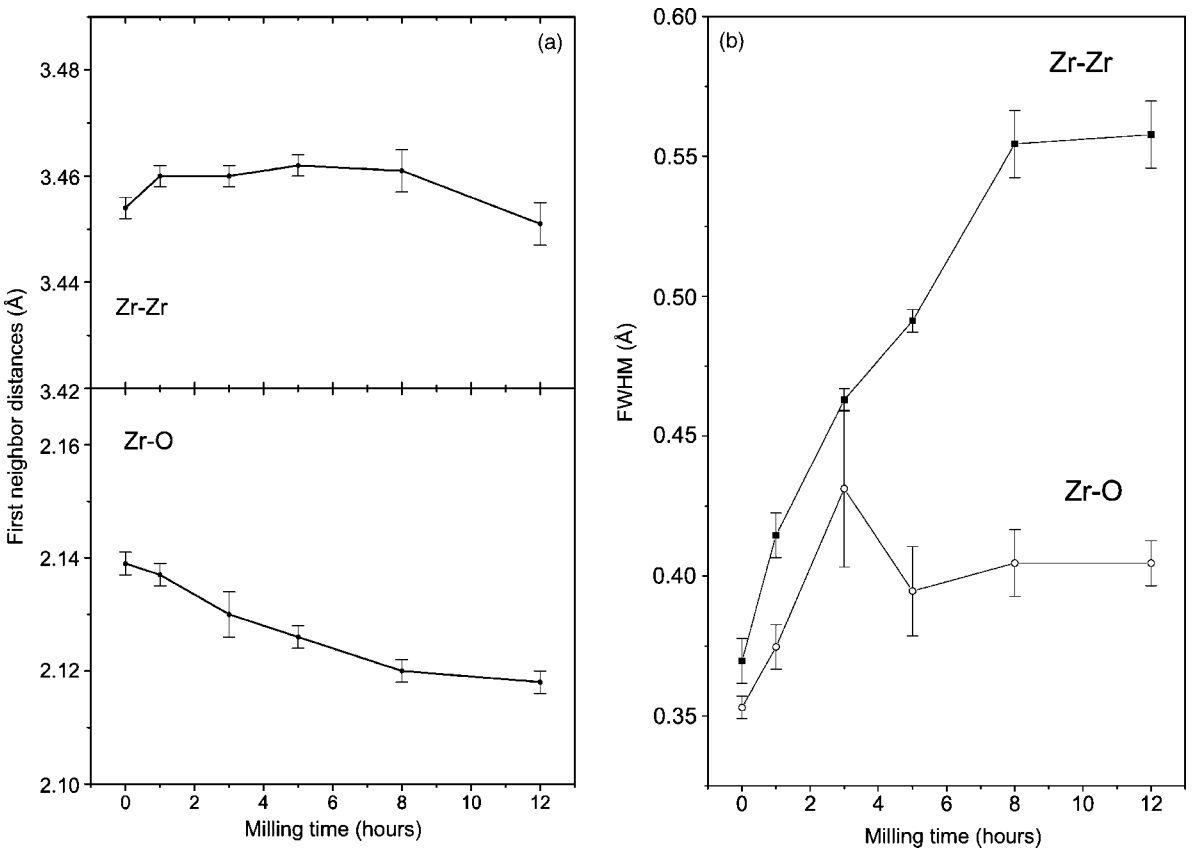

FIG. 5. Positions (a) and FWHM (b) of the first two peaks in the experimental PDFs as a function of milling time. The positions and FWHM are obtained through a Gaussian fit to the experimental data.

tion data, first in reciprocal and then in real space. Initially, we addressed the structure of the precursor: Monoclinic ZrO_2. The experimental powder diffraction data were fit with a model based on structure data taken from literature sources.[19] The fit was done by applying the Rietveld method[20,21] with the help of the program FULLPROF.[22] Results from the Rietveld refinement are shown in Fig. 1. The refined structural parameters agree very well with literature data (see Table I). The atomic PDF obtained from the diffraction data was also fit with the well-known structure data for monoclinic ZrO_2. Similarly to the Rietveld method, the PDF technique employs a least-squares procedure to compare experimental and model data (PDF) calculated from a plausible structural model. The structural parameters of the model (unit-cell constants, atomic coordinates, and thermal factors) are adjusted until the best possible fit to the experimental data is achieved. The progress of the refinement is assessed by computing an agreement factor, R_{wp}:

$$R_{wp} = \left\{ \frac{\sum w_i (G_i^{\text{exp.}} - G_i^{\text{calc.}})^2}{\sum w_i (G_i^{\text{exp.}})^2} \right\}^{1/2}, \qquad (4)$$

where and are the experimental and calculated PDFs, respectively, and w_i are weighting factors reflecting the statistical quality of the individual data points. The best PDF fit achieved for ZrO_2 precursor is shown in Fig. 6, and the corresponding value of R_{wp} is ~21%. The fit was done with the help of the program PDFFIT.[23] The PDF-based fit yielded structural parameters that are in good agreement with the present Rietveld and previous results (see Table I). The agreement well documents the fact that the atomic PDF provides a reliable quantitative basis for structure determination. It may be noted that the agreement factor achieved with the PDF refinement appears somewhat high when compared to the agreement factor, R_{wp}, of 7.6% resulting from the Rietveld refinement of the diffraction data in reciprocal space. This does not indicate an inferior structure refinement (compare the corresponding structural parameters in Table I), but merely reflects the fact that the atomic PDF being fit differs from the corresponding XRD pattern and is a quantity much more sensitive to local ordering in materials. As a result, R_{wp}s greater than 15% are common with PDF refinements even of well-crystallized materials.[15,16,24] The inherently higher absolute value of the goodness-of-fit factors resulting from PDF-based refinements does not affect their functional purpose as residuals function that must be minimized to find the best fit and as a quantity allowing one to differentiate between competing structural models.

Next we approached the experimental diffraction data for the milled samples again with the Rietveld method. Already for the sample milled for 1 h, the Rietveld refinement revealed the presence of a phase with a symmetry higher than monoclinic. We tested the well-known tetragonal and cubic crystalline modifications of zirconia and found that the experimental data are best described by using a mixture of

TABLE I. Structure data for crystalline monoclinic zirconia as obtained by the present Rietveld and PDF refinements and by the independent study of Hann *et al.*[a]

		Present work—Rietveld refinement	Present work—PDF refinement	Hann *et al.*[a]
a(Å)		5.116(3)	5.133(1)	5.1507
b(Å)		5.169(3)	5.182(1)	5.2028
c(Å)		5.284(3)	5.300(1)	5.3156
β(degrees)		98.98(2)	99.19(1)	99.196
Zr	x	0.275(1)	0.277(1)	0.2742
	y	0.038(1)	0.040(1)	0.0389
	z	0.211(1)	0.210(1)	0.2095
O1	x	0.075(3)	0.076(2)	0.0630
	y	0.330(3)	0.335(2)	0.3289
	z	0.346(3)	0.337(3)	0.3476
O2	x	0.461(3)	0.455(2)	0.4491
	y	0.749(2)	0.757(2)	0.7548
	z	0.474(3)	0.477(2)	0.4827

[a]See Ref. 19.

monoclinic and cubic phases. The results of those Rietveld fits are shown in Fig. 1. We found that the relative abundance of the cubic phase increased with milling time, and the XRD data for the sample milled for 12 h are well reproduced with a structure model based almost entirely on the cubic phase of ZrO_2. This outcome of the Rietveld refinement supports the findings of our preliminary analysis of the PDF data that the transformation of crystalline-to-nanocrystalline zirconia is accompanied by a phase transformation involving an increase in the symmetry of atomic ordering. It is well known

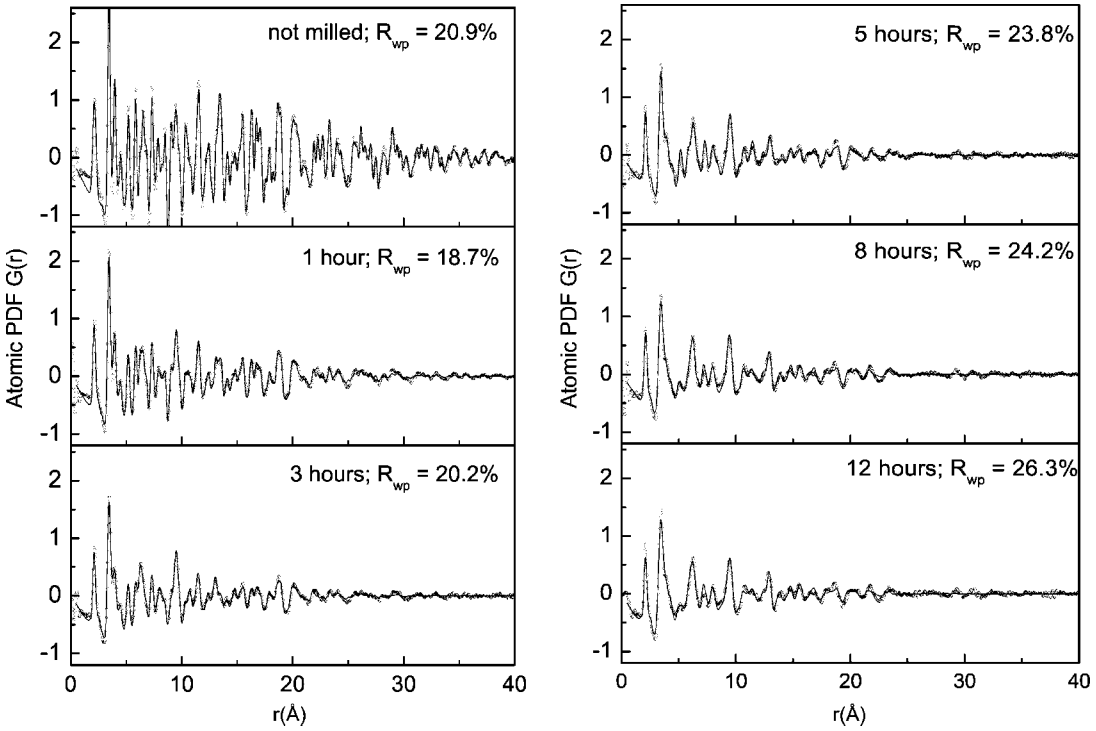

FIG. 6. Experimental (symbols) and model (solid line) PDFs for zirconia milled for different times (given in h). The model PDFs are calculated from a two-phase model.

that the Rietveld method relies mostly on the low-Q (high-intensity) Bragg peaks; ignoring the diffuse component of the diffraction data and, therefore, is sensitive only to the longer-range atomic structure. Thus, the outcome of our Rietveld refinements concerns the longer-range atomic ordering only, clearly showing that it changes from a monoclinic to a cubic type in nanocrystalline zirconia obtained by ball milling. The question about the local atomic ordering remains open and we address it by considering the experimental PDF data. The PDF technique takes into account the *total* scattering, including Bragg peaks and diffuse scattering, and reflects both the longer-range and local atomic structure, as demonstrated in several of our studies on crystalline[14,25] and nanocrystalline materials.[15,16,26] To verify that the longer-range atomic structure of nanocrystalline zirconia is of a cubic type and the local is indeed not, as the results of our preliminary studies suggest, we compared the experimental atomic PDF for the sample milled for 12 h with model ones calculated on the basis of all known polymorphic modifications of ZrO_2, including three atmospheric-pressure (cubic, tetragonal, and monoclinic) and two high-pressure phases (Orthorhombic I and Orthorhombic II.[27–29]) For reference, the monoclinic, tetragonal, cubic, and Orthorhombic I phases may be viewed as modifications of the CaF_2 (fluorite) structure, while the Orthorhombic II phase—of the $PbCl_2$ (cotunnite) structure. When calculating the model PDFs, we adjusted the lattice parameters of the corresponding crystals so that the positions of the peaks in the calculated PDFs at distances longer than 5 Å match as closely as possible those of the peaks in the experimental PDF. In addition, we introduced local structural disorder by artificially enlarging the thermal factors of the atoms in the model atomic configurations and limited the structural coherence length to the experimentally observed one (2–3 nm) by multiplying the model PDFs with a decaying exponent as originally suggested by Ergun *et al.*[30] and, later on, implemented in a similar manner by Gilbert *et al.*[31] The comparison is presented in Figs. 7 and 8. As can be seen in the figures, none of the calculated PDFs reproduces the experimental one over the whole range of r values considered. The low-r range in the experimental PDF (0–5 Å) is reproduced reasonably well only by the model based on the monoclinic structure. The tetragonal structure gives a splitting of the first PDF peak (corresponding to the two different Zr–O distances occurring with this structure) and a shifted second peak (longer Zr–Zr distances). The model PDFs for the cubic and Orthorhombic II structures do not match the experimental one either: The first two peaks in the model PDFs are shifted to higher real-space distances, and the shape of the second peak is not the one the experimental data show. The Orthorhombic I structure describes relatively well the first peak in the experimental PDF but does not reproduce the shape of the second peak. On the other hand, the model PDFs for monoclinic and Orthorhombic II structures do not reproduce the experimental data at higher-r values (5–20 Å). The tetragonal, Orthorhombic I, and cubic-based models, however, reproduce the experimental PDF at higher interatomic distances quite well. The three structures are indeed modifications of the same structural type (CaF_2). Given the disorder introduced in the model atomic configurations, the fact that they exhibit very

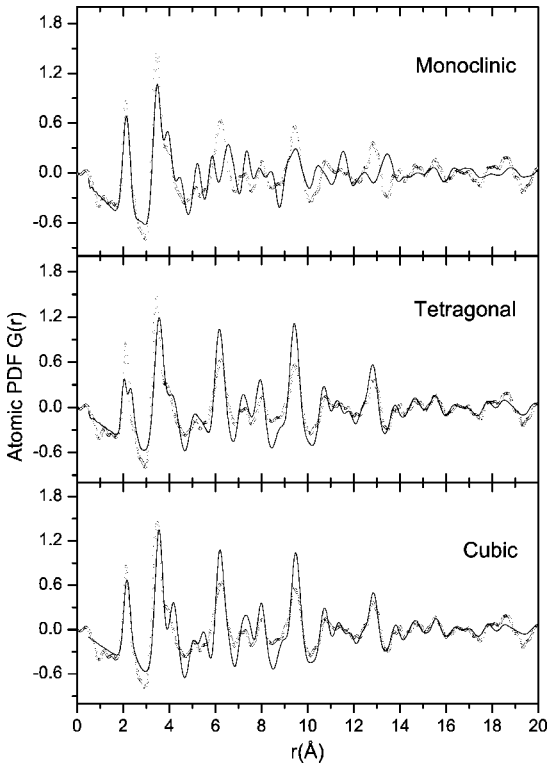

FIG. 7. Experimental PDF for nanocrystalline ZrO_2 (dots) obtained by ball milling for 12 h and model PDFs (solid line) calculated from structure data for three crystalline modifications of ZrO_2 occurring at atmospheric pressure.

similar atomic PDFs at higher-r distances is not a surprise at all. In summary, the PDF modeling confirms the findings of the Rietveld studies that nanocrystalline zirconia possesses a longer-range structure (extending from 5 Å to at least 2–3 nm) that may be described in terms of the CaF_2-type structure having an orthogonal unit cell. Also, it shows that the local atomic ordering (at distances shorter than 5 Å, i.e., within the unit cell) in the material deviates from the longer-range one and resembles that occurring in monoclinic ZrO_2. The question we faced here is whether this picture reflects a single-phase nanomaterial which possesses a cubic-type structure on average but is locally monoclinically distorted, or a nanomaterial composed of two distinct phases, monoclinic and cubic, at the atomic scale. To answer this question, we constructed a two-phase model incorporating both the monoclinic and cubic phases and refined their relative concentration and structure related parameters by fitting the model to the experimental PDF data. The model worked reasonably well, as can be seen in Fig. 6; implying that crystalline monoclinic zirconia is gradually transformed into a two-phase nanocrystalline material with the relative contribution of the cubic phase gradually increasing with milling time. The contributions of these two phases to the model PDF for the sample milled for 12 h are given in Fig. 9(a). The model, however, yielded increasingly worsening reliability factors, R_{wp}, with milling time (see Fig. 6) signaling increased difficulties in representing a material getting more and more nanocrystalline in nature. Also, to achieve the good degree of reproducibility shown in the figure, we had to use very dif-

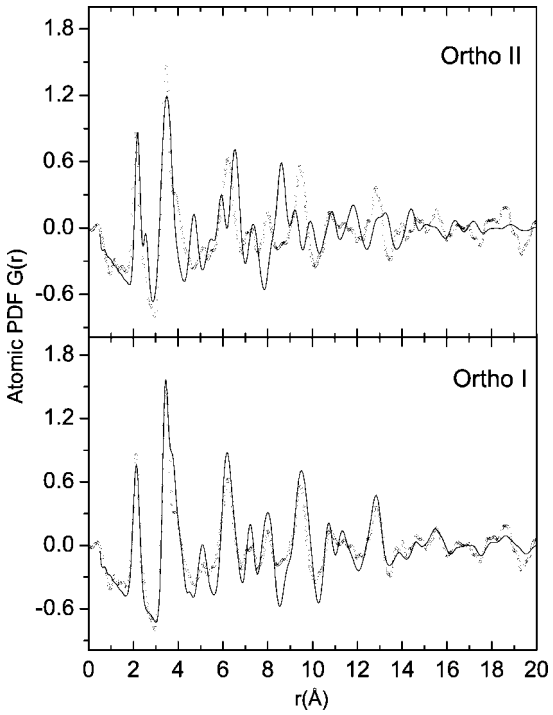

FIG. 8. Experimental PDF for nanocrystalline ZrO_2 (dots) obtained by ball milling for 12 h and model PDFs (solid line) calculated from structure data for two crystalline modifications of ZrO_2 occurring at high pressure.

ferent effective thermal factors, U_{iso} (reflecting the rms fluctuation of the atoms from their average positions), and coherent lengths (size of the coherently scattering domains) for the two different phases. The model refined to a picture suggesting a mixture of extremely small (coherence length $\sim$5–10 Å) and almost perfect ($U_{iso} \sim 0.005$ Å^2) domains/nanocrystallites with monoclinic structure and much more extended (coherence length up to 2–3 nm) and much more distorted ($U_{iso} \sim 0.020$ Å^2) domains/nanocrystallites with cubic structure. This picture is, however, not very likely in our case for the following reasons: The presence of two nanophases should have resulted in a progressively increasing broadening and shifting of the first and second peaks in the experimental PDFs reflecting the increasing relative amount of the cubic nanophase having first-neighbor Zr–O and Zr–Zr distances longer than those in the monoclinic phase. Also, it should have resulted in a measurable change in the area under the first PDF peak reflecting the increasing number of first Zr–O neighbors (seven with monoclinic and eight with cubic zirconia). None of these was observed with our experimental PDF data. Just on the contrary, the experimental first-neighbor distances were found to decrease slightly and the broadening [full width at half maximum (FWHM)] of the first PDF peaks to reach a constant (within the limits of the experimental accuracy) value with milling time (see Fig. 5). The area under the first PDF peak (i.e., the average Zr–O first coordination number) was found to be well preserved as well.

To test the single-phase model, we considered a model atomic configuration based on the unit cell of cubic zirconia, where the local symmetry of the atoms was allowed to relax

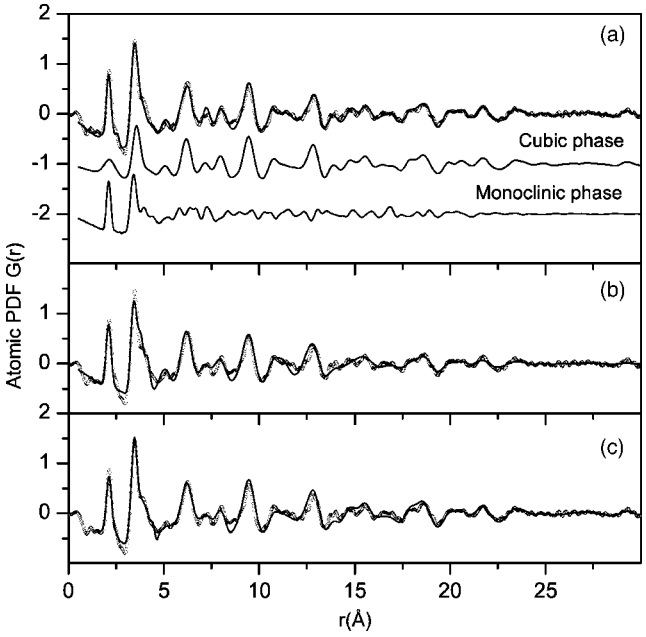

FIG. 9. Experimental PDF for nanocrystalline zirconia obtained by ball milling for 12 h (symbols) and model PDFs (solid line) calculated from (a) a two-phase model incorporating a monoclinic and a cubic phase. The relative contributions of the two phases to the model PDF are also shown displaced vertically for clarity. (b) A single-phase model with a cubic unit cell and local atomic arrangement corresponding to the monoclinic $P2_1/c$ space group. The unit cell contains 12 atoms. (c) A single-phase model of $5\times5\times5$ unit cells of the type described in (b). This supercell model contains approximately 1500 atoms.

to that of the monoclinic space group $P2_1/c$. A model with the atomic arrangement of cubic zirconia (S.G. $Fm\bar{3}m$) shifted by $(1/4,0,1/4)$ with respect to the origin ($m\bar{3}m$) of the cubic lattice was used as a starting point in the simulations. During the simulations, the atoms from the cubic cell were allowed to move off their initial positions; strictly imposing the constraints of the $P2_1/c$ space group. The model performed quite well capturing all important details in the experimental PDF data [see Fig. 9(b)]. It yielded an agreement factor of $R_w = 31\%$, which is only slightly worse than the agreement factor of $R_w = 26.3\%$ achieved with the two-phase model. Note, however, the latter agreement was achieved with a considerably larger number of adjustable parameters (24 for the double-phase versus 16 for the single-phase model). The refined values of the unit-cell constants and atomic coordinates of the single-phase model are summarized in Table II. A fragment of the model is shown in Fig. 10, together with fragments from the monoclinic and cubic structures of crystalline zirconia for comparison. A statistically more representative model was also considered by creating a supercell of $5\times5\times5$ unit cells of the type described above, and refining it against the experimental PDF data. This model reproduced the experimental data even better as was expected [see Fig. 9(c)]. As can be seen in Fig. 10, the single-phase model envisages a nanomaterial with a longer-range structure of a cubic type and local atomic ordering resembling that of monoclinic ZrO_2. The latter is clearly seen

TABLE II. Structure data for nanocrystalline zirconia obtained by ball milling for 12 h. The unit cell is cubic and the atomic positions within it conform to the monoclinic $P2_1/c$ space group.

a(Å)		5.051(1)
Zr	x	0.281(1)
	y	0.009(1)
	z	0.238(1)
O1	x	0.09(1)
	y	0.36(1)
	z	0.38(1)
O2	x	0.47(1)
	y	0.75(1)
	z	0.49(1)

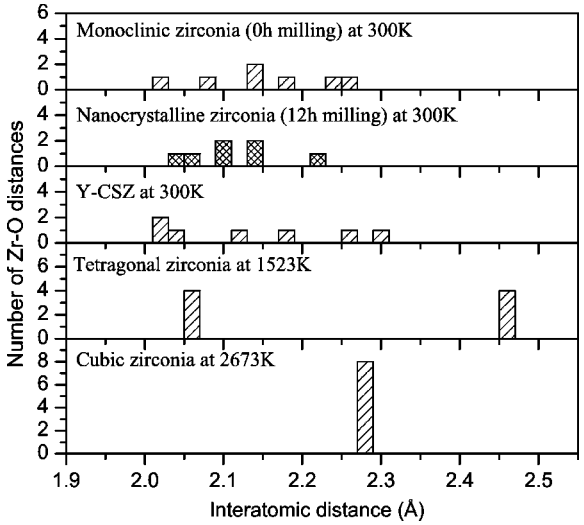

FIG. 11. Distribution of the first-neighbor Zr–O distances in nanocrystalline zirconia obtained by ball milling and different zirconia polymorphs.

in Fig. 11 where the distribution of Zr–O distances in our model atomic configuration (Table II) is compared to those of several crystalline phases of ZrO_2. As our results show, the Zr–O distances in nanocrystalline zirconia spread from approx. 2.0 Å to 2.2 Å, similar to the Zr–O distances in monoclinic ZrO_2 crystal. This picture is distinctly different from the one seen in tetragonal[32] and cubic[33] zirconia where the Zr–O distances group into a two- and single-mode distribution, respectively. A mismatch between the local and average structure, similar to that exhibited by our model for nanocrystalline zirconia, is not an unusual picture and has even been observed with perfectly crystalline materials, such as In–Ga–As semiconductors. These are single-phase materials possessing a long-range cubic structure and local atomic ordering that substantially deviates from it due to the presence of first-neighbor distances (As–In $\sim$ 2.61 Å and As–Ga $\sim$ 2.44 Å) of very different lengths.[14,34]

In summary, the results of our structure studies seem to converge to a picture viewing nanocrystalline zirconia obtained by ball milling as a single-phase material that has inherited its local atomic ordering (within the first coordination shell extending to less than 1 nm) from the parent monoclinic ZrO_2, but has adopted a cubic-type ordering on longer-range distances (longer than a nanometer). The stabilization of the cubic structure is very likely due to the significant structural distortions in the nanophase material introduced by the ball milling process. The situation is indeed very similar to the one realized in Y-stabilized cubic zirconia crystals. Doping monoclinic ZrO_2 with Y results in a crystalline material with a long-range cubic but locally distorted, i.e., less symmetric structure at room temperature.[35] The local distortions are well demonstrated by the broad distribution of Zr–O interatomic distances as obtained by single-crystal studies[35] (see Fig. 11). A similar effect may obviously be achieved by ball milling. Ball milling of monoclinic zirconia introduces structural distortions that reduce the length of structural coherence to a few nanometers, and trigger a change in the type of longer-range order to a cubic one at the

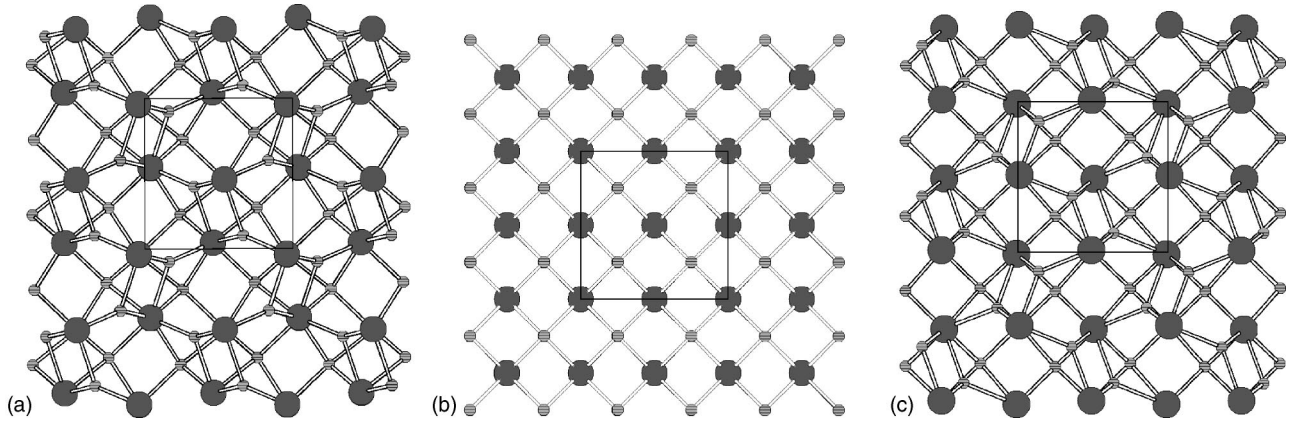

FIG. 10. Fragments from the (a) monoclinic $P2_1/c$ and (b) cubic ($Fm\bar{3}m$) structures occurring with crystalline zirconia; (c) the structure of nanocrystalline zirconia as suggested by the present PDF studies. The latter structure has a cubic unit cell and local atomic ordering of the monoclinic type. The fragment is generated using the structure data shown in Table II. Big circles—Zr atoms, small circles—oxygen atoms. The corresponding unit cells are outlined with thin solid lines.

same time keeping the local atomic structure more or less intact.

V. CONCLUSIONS

Results of our high-energy XRD and atomic PDF studies show that nanocrystalline zirconia obtained by ball milling possesses an atomic-scale structure, which may well be described in terms of a cubic-type lattice and monocliniclike local atomic ordering. Moreover, the structure is given in terms of a small number of sensible parameters, such as unit cells and coordinates of the atoms in it (Table II). This opens up the route to better understanding and possibly improving the structure-related properties of this technologically important material. The results of the study also suggest that the mismatch between the local and longer-range structure is a very important factor in stabilizing the technologically important cubic phase of zirconia at room temperature.

The results of the present study are another demonstration of the ability of the PDF technique to yield 3D structural information for materials of limited structural coherence. The technique succeeds because it relies on total scattering data obtained from the material, and as a result, is sensitive to its essential structural features regardless of crystalline periodicity. The technique probes the bulk of the material and can provide important complementary information not accessible with imaging techniques, such as TEM and atomic force microscopy, which reveal only structural features projected down one axis or a surface.

ACKNOWLEDGMENTS

Thanks are due to M. Beno from APS, Argonne National Laboratory for the help with the synchrotron experiments. The work was supported by the NSF through Grant No. DMR 0304391 (NIRT). The Advanced Photon Source is supported by the DOE under Contract No. W-31-109-ENG-38.

*Electronic address: petkov@phy.cmich.edu

[1] E. C. Subbarao, Ferroelectrics **102**, 267 (1990).
[2] M. Morinaga, J. B. Cohen, and J. Faber, Acta Crystallogr., Sect. A: Cryst. Phys., Diffr., Theor. Gen. Crystallogr. **35**, 789 (1979).
[3] C. J. Howard, R. J. Hill, and B. E. Reichert, Acta Crystallogr., Sect. B: Struct. Sci. **44**, 116 (1988).
[4] V. F. Petrunin, V. V. Popov, Z. Hongzhi, and A. A. Timofeev, Inorg. Mater. **40**, 251 (2004).
[5] R. C. Garvie, J. Phys. Chem. **82**, 218 (1978).
[6] S. Bid and S. K. Pradhan, J. Appl. Crystallogr. **35**, 517 (2002).
[7] D. Michel, L. Mazerolles, P. Berthet, and E. Gaffet, Eur. J. Solid State Inorg. Chem. **32**, 673 (1995).
[8] E. Gaffet, D. Michel, L. Mazerolles, and P. Berthet, Mater. Sci. Forum **235**, 103 (1997).
[9] X. Bokhimi, A. Morales, O. Novaro, M. Portilla, T. Lopez, F. Tzompantzi, and R. Gomez, J. Solid State Chem. **135**, 28 (1998).
[10] E. Djurado, P. Bouvier, and G. Lucazeau, J. Solid State Chem. **149**, 399 (2000).
[11] A. V. Chadwick, M. J. Pooley, K. E. Rammutla, S. L. P. Savin, and A. Rougier, J. Phys.: Condens. Matter **15**, 431 (2003).
[12] H. P. Klug and L. E. Alexander, *X-ray Diffraction Procedures for Polycrystalline Materials* (Wiley, New York, 1974).
[13] Y. Waseda, *The Structure of Noncrystalline Materials* (McGraw–Hill, New York, 1980).
[14] V. Petkov, I.-K. Jeong, J. S. Chung, M. F. Thorpe, S. Kycia, and S. J. L. Billinge, Phys. Rev. Lett. **83**, 4089 (1999).
[15] M. Gateshki, S.-J. Hwang, D. H. Park, Y. Ren, and V. Petkov, J. Phys. Chem. B **108**, 14956 (2004).
[16] V. Petkov, P. N. Trikalitis, E. S. Bozin, S. J. L. Billinge, T. Vogt, and M. G. Kanatzidis, J. Am. Chem. Soc. **124**, 10157 (2002).
[17] V. Petkov, P. Y. Zavalij, S. Lutta, M. S. Whittingham, V. Parvanov, and S. Shastri, Phys. Rev. B **69**, 085410 (2004).
[18] V. Petkov, J. Appl. Crystallogr. **22**, 387 (1989).
[19] R. E. Hann, P. R. Suitch, and J. L. Pentecost, J. Am. Ceram. Soc. **68**, 285 (1985).
[20] H. M. Rietveld, J. Appl. Crystallogr. **2**, 65 (1969).
[21] *The Rietveld Method*, edited by R. A. Young (Oxford University Press, New York, 1996).
[22] J. Rodriguez-Carvajal, Physica B **192**, 55 (1993).
[23] T. Proffen and S. J. L. Billinge, J. Appl. Crystallogr. **32**, 572 (1999).
[24] V. Petkov, S. J. L. Billinge, J. Heising, and M. G. Kanatzidis, J. Am. Chem. Soc. **122**, 11571 (2000).
[25] S. J. L. Billinge, T. Proffen, V. Petkov, J. L. Sarrao, and S. Kycia, Phys. Rev. B **62**, 1203 (2000).
[26] V. Petkov, S. J. L. Billinge, P. Larson, S. D. Mahanti, T. Vogt, K. K. Rangan, and M. G. Kanatzidis, Phys. Rev. B **65**, 092105 (2002).
[27] O. Ohtaka, T. Yamanaka, S. Kume, E. Ito, and A. Navrotsky, J. Am. Ceram. Soc. **74**, 505 (1991).
[28] C. J. Howard, E. H. Kisi, and O. Ohtaka, J. Am. Ceram. Soc. **74**, 2321 (1991).
[29] J. Haines, J. M. Leger, and A. Atouf, J. Am. Ceram. Soc. **78**, 445 (1995).
[30] S. Ergun and R. R. Schehl, Carbon **11**, 127 (1973).
[31] B. Gilbert, F. Huang, H. Zhang, G. A. Waychunas, and J. F. Banfield, Science **305**, 651 (2004).
[32] G. Teufer, Acta Crystallogr. **15**, 1187 (1962).
[33] D. K. Smith and C. F. Cline, J. Am. Ceram. Soc. **45**, 249 (1962).
[34] V. Petkov and S. J. L. Billinge, Physica B **305**, 83 (2001).
[35] N Ishizawa, Y. Matsushima, M. Hayashi, and M. Ueki, Acta Crystallogr., Sect. B: Struct. Sci. **55**, 726 (1999).